CFD Analysis of Swirl Atomizers

Conference Paper · July 2008

DOI: 10.2514/6.2008-5229

3 authors:

Vladimir Bazarov
Georgia Tech Research Institute
38 PUBLICATIONS **579** CITATIONS
SEE PROFILE

Jose Nivaldo Hinckel
National Institute for Space Research
31 PUBLICATIONS **122** CITATIONS
SEE PROFILE

Helcio Villa Nova
Federal University of Itajubá
26 PUBLICATIONS **373** CITATIONS
SEE PROFILE

44th AIAA/ASME/SAE/ASEE Joint Propulsion Conference & Exhibit, July 21-23, Hartford, CT

CFD Analysis of Swirl Atomizers

José N. Hinckel*INPE, São José dos Campos, SP, CEP 12201-970, Brazil

Helcio F. Villa Nova†

INPE, São José dos Campos, SP, CEP 12201-970, Brazil

Vladimir G. Bazarov‡Moscow State Aviation Institute, Moscow 125871, Russia

Liquid swirl injector are widely used in the preparation of the combustible mixtures of high energy density release devices such as rocket engines and jet engines. An ideal, approximate solution to the flow inside the swirl injector was obtained by Abramovich. Many authors, with varying degrees of success, devised methods to improve the accuracy of the Abromovich solution. In this paper we present the results of the analysis of the swirl injector using a CFD code. A large number of parameters were analyzed and the results are compared to original Abramovich solution and some of the improved solutions. The numerical method solves the full Navier-Stolkes equations, including viscous dissipations and admission of the fluid into the swirl chamber though a number of discrete channel orifices. The results obtained from the numerical solution show that, due to the viscous losses in the entrance channels and inside the swirl chamber, the air core at the center is strongly affected; Depending on the range of the parameters analyzed, a liquid column, growing from the bottom of the swirl chamber, fills a large portion air core.

A	Geometric Parameter
b	R/r_c
G	Mass flow rate
n	Number of channels
p	Pressure
r	Radius
S	Cross section area
V	Velocity

Subscripts

a	azimuthal component
c	entrance channel
g	global
h	hydraulic
n	nozzle
r	radial component
tot	total
v	vortex chamber
z	axial component

Symbols

α	Angle of spray
Δp	Pressure drop
μ	Discharge coefficient
ν	Kinematic viscosity
ρ	Density
φ	Fill Coefficient

I. Introduction

The atomization process is widely used in several applications, e.g. spray combustion, spray-painting, spray drying, etc. Spray combustion is used in domestic heating burners, industrial furnaces, gas turbines, diesel engines and rocket engines. For combustion in gas turbine engines for propulsion and power generation applications and aerospace device propulsion, swirl atomizers are widely used for liquid fuel atomization. Swirl atomizers have been found to be the inexpensive and most reliable type of atomizer for fuel injection because of good atomization characteristics and relatively simple geometry. As swirl atomizers offer the advantage in the throttling and give high thrust per element, they have been intensely studied for aerospace propulsion applications over the past 60 years.[1] Other advantages of the swirl injector, as compared to the

*Snr Researcher, INPE, AIAA Member.

†Vis Researcher, INPE

‡Professor and Head, Dynamic Processes Division of the Rocket Engines Chair

jet injector are the good mixing and atomization of the liquids and larger passage dimensions for a given mass flow and pressure drop.

From the operational requirements of the atomizer system it is highly desirable to design atomizers elements that can producer sprays with predetermined droplet size distribution at the desired combustor location (small mean droplet diameters and uniform local air/fuel ratios) to reduce emissions and to yield the uniform heat release from the combustion process.

Another important characteristic of the swirl injector is the rich dynamic behavior, coupling flow perturbations from upstream and downstream, and instabilities arising from the flow inside the injector itself, as described by Bazarov.[2] In these applications, both steady-state and dynamic characteristics of the injector have been of great interest to predict bulk performance and to understand instability mechanism related to the dynamic response of engines.

The flow inside a swirl atomizers is predominantly turbulent and contains regions of recirculation. The internal flow characteristics in swirl atomizers are important because they govern the thickness of the sheet formed at the discharge orifice.

The swirl atomizer is composed mainly of tangential entrance channels, a swirl chamber and an exit nozzle. Figure 1 shows a schematic of a swirl atomizers. High-pressure liquid is forced to enter a swirl chamber through tangential orifice inlet at the outer wall such that the liquid has a swirling motion. Due to high swirl velocity, an air core is formed around the centerline of the atomizer. The liquid exits through a small orifice in the form of a hollow nearly conical sheet. Further downstream the thin liquid sheet becomes unstable and breaks up into spray of droplets. The mean droplet diameter (which is roughly proportional to the square root of the film thickness) and the spray angle are the two important parameters governing atomizer performance.

The flow behavior inside a swirl atomizers is very complex and difficult to describe. Additionally, the shape and the location of the liquid-air interface is unknown and must be determined as part of the solution. This poses significant difficulties in the solution of the flow in a swirl atomizers. Analytical, numerical and experimental methods have been used to to determine the flow conditions inside the swirl injectors. The first analytical solution was formulated by Abramovich. This solutions is described in,[3] [4, pp. 4-9] and [1, pp. 252-271].

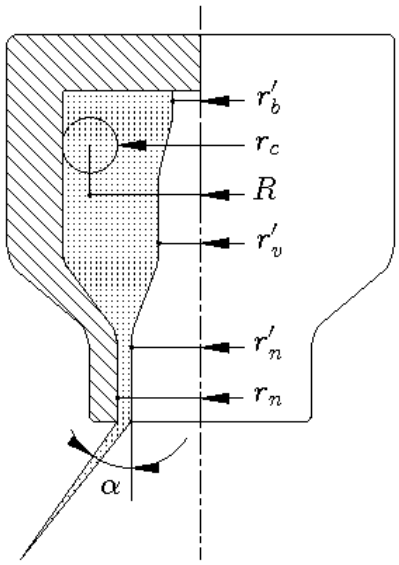

Figure 1. The main geometric characteristics of the swirl injector.

Bavyel[1] describes at length the atomization phenomena and underlying physics. Khavkin[4] describes the extensive work of many researchers, related to theoretical as well as experimental investigation of swirl injectors, mainly in scientific institutions of the former Soviet Union.

Further developments on the effect of other geometric parameters were primarily based on experimental measurements. As described in Chinn,[5] Xue[6] and Xue[7] several semi-empirical correlations were developed that took into account the effect of length and diameter of the tangential inlet orifice diameter and that of exit orifice. However, there remain discrepancies in the predictions of film thickness and spray cone angle made by available correlations. Furthermore, not all geometric parameters of the atomizer have been considered in available correlations. One of the most important parameters of swirl atomizer internal flow is the size of the air core in the outlet orifice, from which may be determined the operating liquid film thickness. From the film thickness, liquid velocities and liquid and ambient gas properties the spray droplet structure may be determined.

The Abramovich solution yields quite accurate results for low viscosity fluids and moderate and high mass flows. To obtain more reliable results for a wider range of flow parameters, the full Navier-Stokes equation must be solved. No general solution for these equations with the complex geometry of the swirl injector is available.

The numerical solution of the flow inside the injector gives very accurate results for the steady state flow characteristics and also for the calculation of the parameters used in the analysis of the dynamic behavior of the injector. In this paper we present the results for a range of parameters covering flow regimes where

approximations used in the analytical solution are valid, and flow regimes where viscosity effects and other geometrical characteristics cause deviations from the ideal flow.

Recent computational efforts in this area have advanced the knowledge on several fronts: internal flow characteristics, film thickness measurement, hollow-cone spray, dynamic behavior of liquid sheets. Computational Fluid Dynamics (CFD) provide additional insight into the characteristics of the internal flow of swirl atomizers. Numerical studies of the internal flow have often been performed assuming axisymmetric flow and single phase. The main difficulty in the numerical simulation of the flow in a swirl injector is the accurate tracking of the liquid/air interface.

A three-dimensional two-phase fluid flow simulation is presented, where the flow inside a swirl injector is studied. The simulation gives good qualitative and numerical results. The gas-liquid flow was simulated using the homogeneous two-phase flow model in CFX-11. The VOF method, described in[8] is used for the two-phase model.

To validate the numerical commercial CFD code, experimental measurements of flowfield in the atomizer are required. However, typical swirl atomizers used in aerospace device propulsion are very small (nozzle diameter $\leq$ 5mm), and measurements of flowfield inside the atomizer are extremely difficult. To overcome this difficulty, the validated computational code was based under numerical and experimental studies available.

II. The Abramovich solution

The main results of ideal swirl flow solution are presented here for purposes of comparison and for completeness. The basic geometry of the swirl injector is shown in Figure 1. The "primed" variables refer to the gas core.

The main hypotheses in the ideal solution of the swirl injector are:

- There are no friction losses.
- The angular momentum of the flow inside de swirl chamber is constant.

From the first hypothesis it follows that the total velocity defined by

$$V_{tot} = \sqrt{\frac{2\Delta p}{\rho}} \tag{1}$$

is constant throughout the flow field. Δp is the pressure drop across the injector, i.e. the difference between the entrance reservoir pressure and the ambient exit pressure.

As the liquid moves towards the central region of the injector, its azimuthal velocity increases and the pressure decreases. The axial velocity increases from the bottom of the vortex chamber to the nozzle exit. The modulus of the velocity, $V = \sqrt{V_r^2 + V_a^2 + V_z^2}$, and the local static pressure, p, must satisfy the relation $V_{tot} = p + \rho V^2/2$. The surface of revolution in the central region of the injector where the static pressure, p, is equal to the exit ambient pressure defines the free surface of the liquid. The interior of the surface may be filled with vapor of the working fluid if the exit ambient is vacuum, air at ambient pressure for injection into the atmosphere, or combustion gas product for injection into a combustion chamber.

The diameter of the surface of revolution defining the free surface of the liquid increases from the bottom towards the exit section of the injector. At the bottom of the injector, where $V_z = V_r = 0$, the azimuthal component of the velocity is maximum. In the vortex chamber the axial and radial components of the velocity are low and the azimuthal velocity slightly lower than at the bottom of the injector. In the nozzle region where the area of the cross section of the liquid flow is small the axial velocity is high and the azimuthal velocity decreases further.

To obtain a simple analytical solution a further hypothesis is made; that the axial velocity is uniform in each cross section of liquid flow along the axis of the injector.

The main parameter of the swirl injector is the geometric characteristic A, defined by:

$$A = \frac{\pi R r_n}{S_c} = \frac{R r_n}{n r_c^2} \tag{2}$$

The second part of the equality in equation 2 is valid only if the the entrance channels are circular.

Other important parameters of the swirl injector are: (i) the fill coefficient, φ, the ratio of the area of the cross section of the liquid flow in the nozzle to the cross section of the nozzle; (ii) the discharge coefficient,

μ; and (iii) the angle of the exit conic liquid sheet, α. All these paramenter are directly related to A by the following formulas:

$$A = \frac{(1-\varphi)\sqrt{2}}{\varphi\sqrt{\varphi}} \tag{3}$$

$$\mu = \varphi\sqrt{\frac{\varphi}{2-\varphi}} \tag{4}$$

$$\tan\frac{\alpha}{2} = \frac{2\sqrt{2}(1-\varphi)}{\sqrt{\varphi}(1+\sqrt{1-\varphi})} \tag{5}$$

The mass flow of the injector is given by:

$$\dot{m} = \mu S_n\sqrt{2\rho\Delta p} \tag{6}$$

III. "Engineering" the Abromovich solution

The solution presented above is a good starting point to obtain the main dimensions of the injector. The accuracy of the mass flow rate and the angle of the spray cone is good for mass flow rates above 5 g/s and low values of the parameter b, defined later in this paper.

The deviations from the ideal solution for low mass flow rates, are mainly due to viscous losses, which become more important as the Reynolds number of flow decreases. Another source of error for low mass flow rate is the loss of dimensional accuracy of the machining of entrance channel and exit nozzle.

The main effect of the viscosity is the loss of total pressure between the entrance and exit sections of the injector. It is interresting to divide the loss of total pressure three regions: the entrance channels, the vortex chamber and the exit nozzle.

In the entrance channels the loss of total pressure is due mainly to the viscous dissipation associated with shear stresses in the boundary layer near the channel walls.

In the vortex chamber we also have the viscous dissipation in the wall boundary layer. Additional losses occur in the interior of the flow due the shear stresses between two layer at different radial positions.

In the exit nozzle we also have the losses associated with the wall boundary layer and shear stresses between concentric layers.

We can define different Reynolds numbers for the injector; (i) a global Reynolds number, $Re_g = (V_{tot}d_n)/\nu$, (ii) a Reynolds number for the entrance channels, $Re_c = 4G/(\pi\rho\nu\sqrt{n}d_c)$ and a Reynolds number for the exit nozzle, $Re_n = (V_{tot}d_h)/\nu$, where $d_h = r_n(1-\sqrt{\varphi})$ is the hydraulic diameter for the flow in the exit nozzle.

Depending on the flow conditions, and on the geometry of the injector, the relative importance of losses occurring in the different portions of the injector may vary. The effect of the losses in the different portions of the injector on the main operation characteristics of the injector are also different. Viscous dissipation in the entrance channels have the effect of decreasing the mass flow rate for a given pressure drop. Viscous dissipation inside the swirl chamber increases the mass flow rate for a given pressure drop. The viscous dissipation occurring in the exit nozzle have the effect of decreasing the mass flow rate and reducing the angle of the spray cone.

The apparently contradictory behavior of the viscous losses inside the swirl chamber increasing the mass flow rate, for a given pressure drop, is explained in the following way: The loss of total pressure due to viscous dissipation decreases the azimuthal velocity and reduces the diameter of the gas core, which in turn increases the thickness of the liquid film in the exit nozzle and the fill coefficient of the nozzle. The net effect is the decrease of the total flow resistance of the swirl chamber and the exit nozzle.

Since the pressure drop of the swirl chamber is usually several times the pressure drop of the entrance channels, the overall effect of viscous dissipation in the swirl injector is the increase of the mass flow for a given pressure drop, since increased flow resistance of entrance channel is compensated for by the decreased resistance of the swirl chamber and exit nozzle.

Vasiliev [9, pp 175-214] describes experimental results comparing the measured discharge coefficient with the calculated values according to the ideal solution. An increase of up to 300% is observed for some combinations of geometrical and flow parameters. Bayvel[1] and Khavkin[4] also present and discuss

the phenomena responsible for the discrepancies observed in the discharge coefficient, spray cone angle and azimuthal uniformity of the mass flow rate.

Khavkin [4, pp 35-48] describes an approximate analytical solution taking into account the effects of viscosity and claims high accuracy of results for a wide range of parameter. Experimental results for more than 100 injector geometries are presented to back up the claimed accuracy.

Khavkin[4] describes a simplified procedure to include the effects of viscosity in sizing of injector. The results obtained from this procedure are used to compare with the ideal swirl injector and the CFD calculations.

One interresting aspect of the swirl injector design is the uniformity of the flow at the inlet of the tangential entrance channels. The mass flow rate of each entrance channel is governed by pressure drop across the channel. A very small difference of total pressure at the entrance of the channels may cause a large difference of mass flow from channel to channel. this difference may propagate to the exit nozzle and cause a nonuniform mass flow distribution in the azimuthal coordinate.

The reason for this behavior is that the difference of total pressure is allocated only to the entrance channel and not distributed between entrance channel, swirl chamber and exit nozzle.

IV. Description of the CFD solution

The CFD tool used was the Ansys CFX package. This package can handle compressible and incompressible fluid flows, laminar and turbulent flow regimes in elliptic, parabolic and hyperbolic domains. The continuity, momentum and energy equation are solved in a discretized finite volume grid. The momentum equation includes turbulent flux terms in addition to the molecular diffusive flux terms. Turbulence models close the Reynolds-averaged equations by providing models for the computation of the Reynolds stresses and Reynolds fluxes. The solutions presented in this paper used the two-equation $\kappa - \epsilon$ turbulence model in CFX-11. Three regions can be distinguished in the injector: entrance channels, vortex chamber and exit nozzle, each one with distinctive characteristic velocity and length. For each region a corresponding Reynolds number may be defined. For all operating conditions and geometric characteristics of injector used in this work, the entrance channel Reynolds number has the smallest value; of the order of 10^4. Therefore the flow regime was considered to be turbulent in the entire flowfield.

The pseudo-transient iterative solution started with an initial condition where the entire flow domain was filled with stationary liquid. The boundary conditions imposed were zero static pressure at the exit section and a total pressure of 5 bar at the inlet section of the tangential entrance channels.

An orthogonal adaptive mesh was used with O-grid type blocks. The number of nodes was approximately 68000.

Many methods exist to simulate two-phase flow-fields and a brief examination of the currently available techniques can be found in Steinthorsson and Lee.[8] In this study, the VOF method, implemented in the CFX package, is used to simulate the flow of water and water vapor. The establishment of a central gas core was simulated using a Rayleigth-Plesset model.

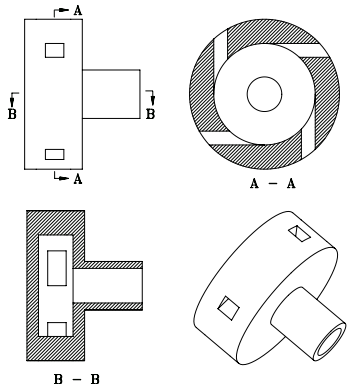

Figure 2. Geometry of the test injector

The geometry of the injector is shown in Figure 2. The cross section of the vortex chamber in the axial plane is retangular without a conical transition section to the nozzle. The entrance channel cross section is retangular with the height larger than the width.

The number of channels varied from 2 to 6. Geometric data for the injector are presented in table 1. A is the geometric parameter, R Radial distance of entrance channels, r radius of the nozzle, H height of the vortex chamber, n the number of entrance channels, w and h, the width and height of the entrance channels.

The analytical solution to the flow in the swirl injector has been used with good results to obtain the main characteristics of the flow: the mass flow rate, and angle of spray cone.

A large number of experiments has also been realized. The comparison of analytical calculations and experimental results shows good agreement over a limited range of geometrical and flow parameters.

The experimental approach is limited by a number of factors: (i) The number of parameter involved is large and the ranges are wide. (ii) The control of the experimental conditions is very difficult to realize. (iii) The manufacturing and inspection of the test specimens and experimental setup are time and resource consuming, with limited possibilities of automation.

The CFD approach in turn can be very effectively automated. Once the basic geometry has been established, covering the geometrical and operating parameters is easily realized by compact and easily written scripting programs.

The geometrical configuration of the injector, the flow conditions and fluid properties of the injector element are well within the domain where the numerical solution obtained with standard algorithms has very good accuracy, does not require very large memory or long CPU time.

V. The parameters and ranges investigated

The ideal solution is governed entirely by the geometrical parameter, A. In the real world a large number other parameter may have influence on the mass flow characteristics of the injector: the length and cross section of the entrance channels, the number of entrance channels, the length of the swirl chamber, transition section and exit nozzle.

The solution was obtained for 4 values of the parmeter A: 1, 2.5, 5 and 30. The analysis of the flow conditions and a number of experiments presented in[9] verifies the influence of other parameter delimiting accuracy and the range of validity of the ideal solution, the mass flow rate of the injector and the parameter b. Parameter b is the ratio of the radial distance of the entrance channels to the radius of the entrance channels. Three values of parameter b were investigated: 2, 5 and 10. For each combination of parameters A and b we also investigated different values of the mass flow rate; in the vicinity of 2 g/s, 5 g/s and 30 g/s.

A	b	R	r	H	n	w	h
		[mm]	[mm]	[mm]		[mm]	[mm]
1	2	0.46	0.23	0.92	2	0.37	0.45
1	2	0.73	0.36	1.46	2	0.58	0.72
1	2	0.89	0.89	1.78	4	0.71	0.88
1	5	1.44	0.23	1.15	4	0.60	0.57
1	5	1.52	0.36	1.21	6	0.49	0.60
1	5	3.72	0.89	2.97	6	1.19	1.46
1	10	3.84	0.23	1.54	6	0.61	0.75
1	10	1.52	0.36	1.21	6	0.49	0.60
1	10	14.87	0.89	5.95	6	2.38	2.92
2.5	2	0.25	0.31	0.49	2	0.2	0.24
2.5	2	0.39	0.49	0.78	2	0.31	0.38
2.5	2	0.95	1.19	1.91	2	0.76	0.94
2.5	5	1.54	0.31	1.23	2	0.49	0.60
2.5	5	1.22	0.49	0.97	4	0.39	0.48
2.5	5	1.99	1.19	1.59	6	0.64	0.78
2.5	10	3.08	0.31	1.23	4	0.49	0.60
2.5	10	3.25	0.49	1.30	6	0.52	0.64
2.5	10	7.95	1.19	3.18	6	1.27	1.56
5	5	0.96	0.38	0.77	2	0.31	0.38
5	5	1.52	0.61	1.22	2	0.49	0.60
5	5	1.86	1.49	1.49	4	0.60	0.73
5	10	1.92	0.38	0.77	4	0.31	0.38
5	10	3.04	0.61	1.22	4	0.49	0.60
5	10	4.97	1.49	1.99	6	0.79	0.98
30	10	1.19	0.72	0.48	2	0.19	0.23
30	10	1.89	1.13	0.76	2	0.30	0.37

Table 1. Geometry of injectors

For each combination of parameters we calculated the ideal solution, the solution corrected for the effects of viscosity according to formulas presented in[9] and the numerical solution. The pressure drop from entrance channel to nozzle exit was 0.5 MPa in all calculations.

VI. Analysis of the results

The results are presented in Table 2. The first two columns contain all combinations of parameter A and b. Columns 3-5 contains the results for mass flow rate in the vicinity of 2 g/s. Columns 6-8 and 9-11 to the right show the solution for 5 g/s and 30 g/s respectively.

The ideal solution mass flow is in columns headed by $\dot{m}_{id}$. The viscosity corrected solution, $\dot{m}_{cor}$ and numerical solution, $\dot{m}_{num}$ are normalized by the ideal mass flow rate. As expected the largest deviation were observed for low mass flow rate, high values of parameters b and A. It is interresting to note that in all cases the viscosity correction increased the mass flow rate. The numerical results were in some cases lower than the ideal solution.

A	b	$\dot{m}_{id}$	$\frac{\dot{m}_{cor}}{\dot{m}_{id}}$	$\frac{\dot{m}_{num}}{\dot{m}_{id}}$	$\dot{m}_{id}$	$\frac{\dot{m}_{cor}}{\dot{m}_{id}}$	$\frac{\dot{m}_{num}}{\dot{m}_{id}}$	$\dot{m}_{id}$	$\frac{\dot{m}_{cor}}{\dot{m}_{id}}$	$\frac{\dot{m}_{num}}{\dot{m}_{id}}$
		[g/s]			[g/s]			[g/s]		
1.0	2.0	2.30	1.10	0.74	5.66	1.01	0.71	34.47	1.00	0.81
1.0	5.0	2.30	1.03	1.24	5.71	1.03	0.97	34.43	1.02	0.87
1.0	10.0	2.28	1.13	1.35	5.71	1.03	0.97	34.45	1.11	1.47
2.5	2.0	2.34	0.99	0.68	5.82	0.99	0.70	34.94	1.00	0.74
2.5	5.0	2.33	1.13	1.40	5.89	1.04	0.80	34.96	1.01	0.84
2.5	10.0	2.33	1.17	1.79	5.89	1.16	1.22	34.79	1.13	1.18
5.0	5.0	2.15	1.10	0.95	5.45	1.09	0.95	32.46	1.01	0.82
5.0	10.0	2.15	1.27	1.31	5.45	1.25	1.27	32.26	1.12	1.00
30.0	10.0	1.52	1.33	1.07	3.81	1.28	1.08			

Table 2. Summary of calculated data

Table 3 presents the data for the losses of total pressure in the vortex chamber, ΔP_{vc}, and the exit nozzle, ΔP_n. The tabulated data are relative to the total entrance pressure. For most geometries the losses of total pressure in the vortex chamber were higher than in the nozzle. The calculated value of loss of total pressure across the injector was very high, varying from 20% to 94%.

A	b	$\dot{m}_{id}$	ΔP_v	ΔP_n	$\dot{m}_{id}$	ΔP_v	ΔP_n	$\dot{m}_{id}$	ΔP_v	ΔP_n
		[g/s]			[g/s]			[g/s]		
1.0	2.0	2.30	0.60	0.10	5.66	0.61	0.09	34.47	0.13	0.14
1.0	5.0	2.30	0.36	0.17	5.71	0.43	0.13	34.43	0.50	0.11
1.0	10.0	2.28	0.09	0.29	5.71	0.43	0.13	34.45	0.12	0.19
2.5	2.0	2.34	0.37	0.22	5.82	0.33	0.22	34.94	0.28	0.21
2.5	5.0	2.33	0.63	0.10	5.89	0.53	0.14	34.96	0.29	0.20
2.5	10.0	2.33	0.47	0.15	5.89	0.53	0.11	34.79	0.54	0.11
5.0	5.0	2.15	0.63	0.13	5.45	0.63	0.13	32.46	0.301	0.30
5.0	10.0	2.15	0.57	0.14	5.45	0.59	0.15	32.26	0.45	0.19
30.0	10.0	1.52	0.75	0.19	3.81	0.72	0.21			

Table 3. Relative losses of total pressure in the vortex chamber and nozzle

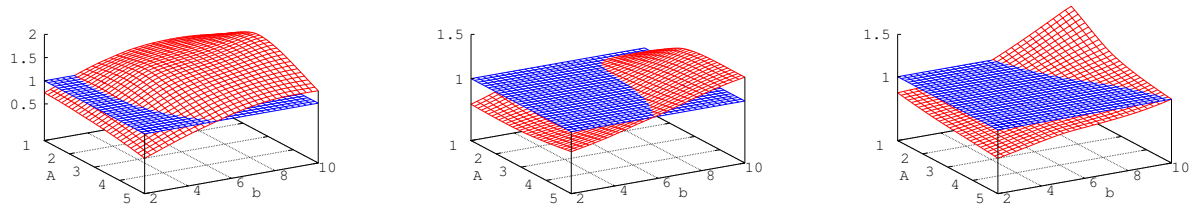

(a) 2gps (b) 5gps (c) 30gps

Figure 3. Ratio of numerical mass flow rate to ideal mass flow rate

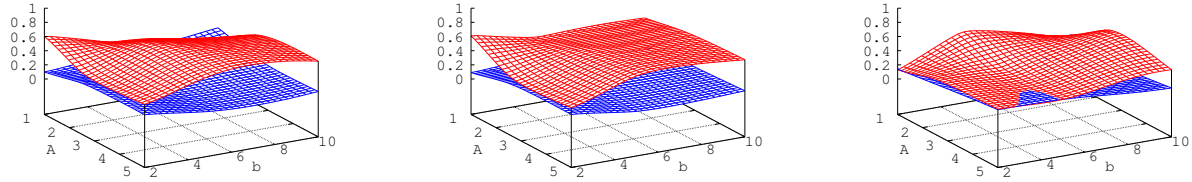

(a) 2gps (b) 5gps (c) 30gps

Figure 4. Relative losses of total pressure in the vortex chamber (red) and exit nozzle (blue)

Figures 3 and 4 are 3-D plots of data in Tables 2 and 3.

Parameters A and b are the coordinate axes. One plot is presented for each value of the ideal mass flow rate. The data plotted in 2 are the ratios of numerical value of mass flow rate divided by the ideal mass flow rate (red mesh lines). The blue mesh line is the plane at unitary height. It is clear from the plot that the numerical mass flow rate is higher than the ideal mass flow rate over large part of the ranges of parameters A and b for low mass flow rate injectors. For higher mass flow rates the numerical value is less than the ideal value for large portion of the domain in the A, b parameters.

The data obtained from the numerical solution are useful for illustrating a number of phenomena taking place inside the swirl injector. Using the rich post-processor interface we can visualize the pressure, velocity and phase distribution in any section of the injector.

From the phase flow data it is possible to observe the size and localization of the gas core in the center region of the injector. Figure 5 shows the phase distribution for different sets of parameters. It is interesting to notice that for some sets of parameteres, the gas core disappears near the bottom wall of the injector. The mechanism responsible for the colapse of the vortex in this region is the loss of angular momentum due to friction losses near the bottom wall and between concentric layers near the axis of the vortex. The collapsed vortex is filled by a column of uniformly rotating liquid. Friction losses near the bottom of the the injector are greater because of the long residence time of the liquid in this region.

This situation contrasts markedly with the ideal solution where a gas core is always present.

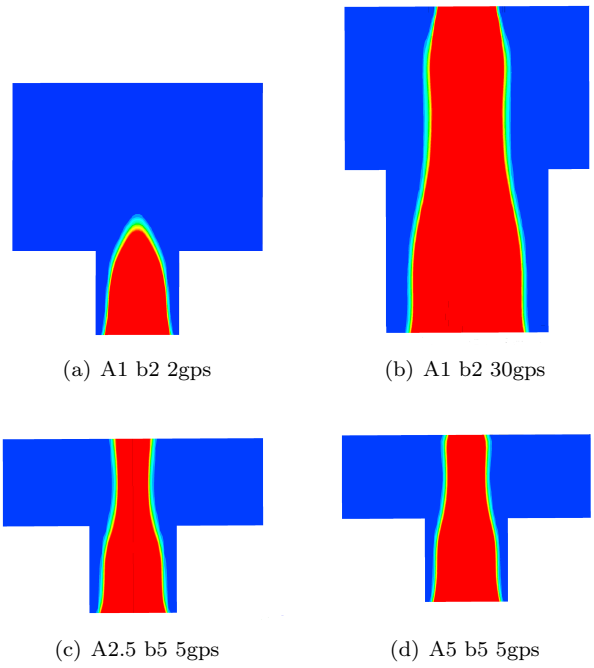

(a) A1 b2 2gps (b) A1 b2 30gps

(c) A2.5 b5 5gps (d) A5 b5 5gps

Figure 5. Vapor fraction

Figure 6 shows the static and total pressure in a meridional section of the injector. The losses of total pressure occur in the wall boundary layers and in the central region of the injector. The mechanism for the losses of total pressure is viscous dissipation. Near the walls the dissipation occurs in the boundary layer. A strong gradient of the total pressure along the radial direction is also observed in the central region of the vortex chamber. The shear movement between concentric layers in this region is associated with the angular momentum balance as the fluid moves toward the axis of the vortex chamber.

The general trend observed is that the losses of total pressure are higher in the vortex chamber than in the exit nozzle, although some combinations of extreme values of A and b may show this condition reversed. For the same combination of parameters A and b it is observed that the losses of total pressure decrease as the moss flow rate of the injector increases.

The velocity flow field is substantially different from conditions considered in derivation of the ideal solution. The inward radial movement of the flow inside the vortex chamber is confined to thin layers near the the top and lower wall of the vortex chamber 8. In the central region of the vortex chamber the radial velocity of the fluid is positive, i.e. the fluid moves outward. Rainbow rendered sections of the velocity flow field in the injector are show in 7. In (a) of Figure 7 the coordinate axis points to the right and the

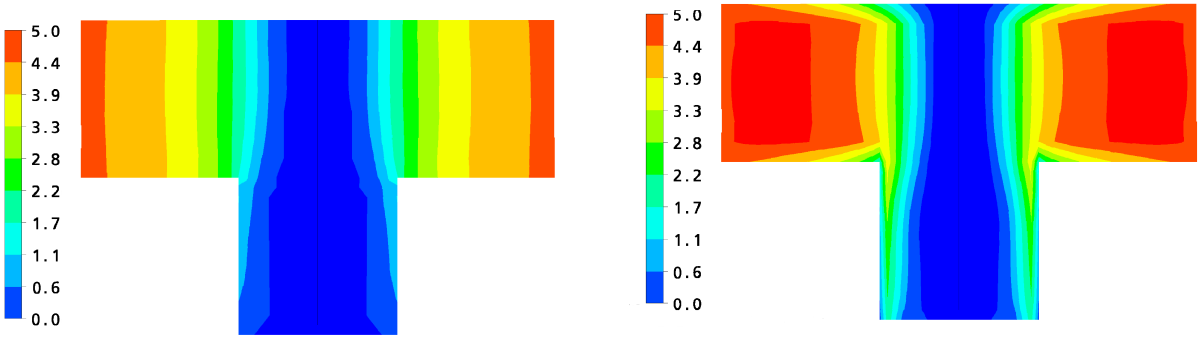

(a) Static Pressure (Bar) A = 2.5, b = 5 (b) Total Pressure (Bar) A = 2.5, b = 5

Figure 6. Static pressure and total pressure

velocity field is anti-symmetric with respect to the center line of the injector. In (b) the coordinate axis points downwards. In (c) the field plotted is the modulus of the velocity.

Figure 8 shows the velocity field. The radial velocity is plotted along a line from the top wall to the bottom wall. The line is located at a radial position interior to the entrance channel. The azimuthal velocity field is plotted along a radial line on a plane located at half the height of the vortex chamber. The axial velocity field is plotted along radial lines located at half the height of the vortex chamber and near the top and bottom walls of the vortex chamber. The ideal solution is included for comparison.

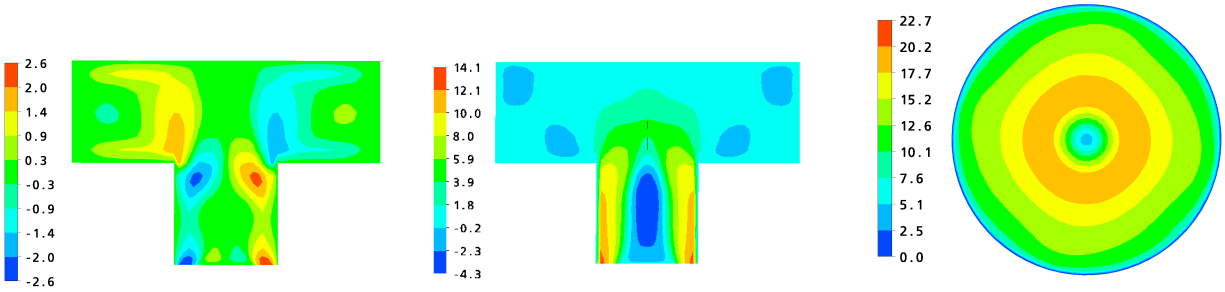

(a) Radial velocity (m/s) (b) Axial velocity (m/s) (c) Modulus of velocity (m/s)

Figure 7. Velocities components contours

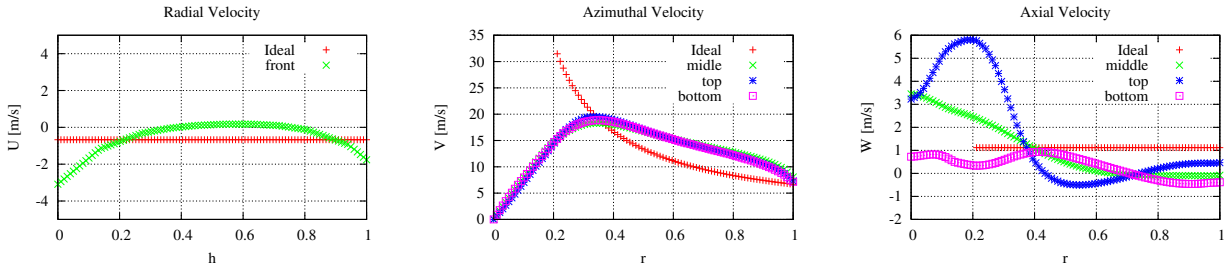

(a) U (b) V (c) W

Figure 8. Velocities

VII. Conclusion

In this paper we present a CFD study of liquid swirl injector. A wide range of parameters A b and mass flowrate is covered. The main purpose of the work is to determine the accuracy of the original Abramovich solution and other "improved" and "corrected" solutions. In the Abramovich solution the flow coefficient of the injector and the angle of conical spray sheet depends only on parameter A. The "improved" solutions tweaked the Abramovich solution to take into account the effects of viscosity in the vortex chamber. The choice of parameters A and b was made to have a comparison with experimental data presented in [9, p.190]. According to these data the discharge coefficient of the injector may vary by up to a factor of 4 by changing b from 3.29 to 14.75 for a value of A in the vicinity of 4.5. The experimental data include the variation of the mass flowrate, by varying the injector pressure drop from 0.01 MPa to 1 MPa.

The CFD results agree qualitatively with the experimental results, but the magnitude of the variation of the flow coefficient is much smaller. One possible reason for the difference in the results is that the experimental data were obtained with large mass flow injectors. To resolve this difference the CFD simulation must be run with the same geometry used in the experimental setup. In this way we can verify the accuracy of the numerical solution; which can then be applied to geometries more difficult to test experimentally.

It should be stressed that the boundary conditions used in this simulation were 0.5 MPa total pressure at the injector entrance and 0.0 Pa static pressure at the exit of the injector, which corresponds to injection into vacuum ambient. By changing the boundary conditions to a gaseous pressure condition at the exit and

a correspondingly higher total pressure at the entrance the geometry of the gas core and the mass flow rate were not affected.

One interesting result was the large losses of total pressure in the vortex chamber and exit nozzle over the range of the parameters tested. Surprisingly this losses of total pressure did not have a large effect on the discharge coefficient of the injectors.

References

[1]Bayvel, L. and Orzechowski, Z., *Liquid Atomization*, Taylor & Francis, 1993.

[2]Bazarov, V. G. and V.Yang, "Liquid-Propellant Rocket Engine Injector Dynamics," *Journal of Propulsion and Power*, Vol. 14, No. 5, 1998, pp. 797–806.

[3]Bazarov, V. G., Yang, V., and Puri, P., *Liquid Rocket Thrust Chambers: Aspects of Modeling, Analysis, and Design*, Vol. 200 of *Progress in Astronautics and Aeronautics*, chap. 5: Design and Dynamics of Jet and Swirl Injectors, American Institute of Aeronautics and Astronautics, Inc., 2004.

[4]Khavkin, Y. I., *The Theory an Practice of Swirl Atomizers*, Taylor & Francis, 2004.

[5]Chinn, J. J., "ILASS - Europe 2007," *Proceedings of the 21st ILASS-Europe Meeting 2007*, ILASS, Mugla, Turkey, 2007.

[6]Xue, J., Jog, M. A., Jeng, S. M., Steinthorsson, E., and Benjamin, M. A., "Effect of Geometric Parameter on Simplex Atomizer Performance," *AIAA Journal*, Vol. 42, No. 12, 2004, pp. 2408–2415.

[7]Xue, J., Jog, M. A., Jeng, S. M., Steinthorsson, E., and Benjamin, M. A., "Influence of Geometry on the Performance of Simplex Nozzles under Constant Pressure Drop," *ILASS Americas*, Madison, WI, USA, May 2002.

[8]Steinthorsson, E. and Lee, D. M., "Numerical Simulations of Internal Flow in a Simplex Atomizer," *ILASS-Americas*, Irvine, CA, 2000.

[9]Vasiliev, A. P., Kurpatenkov, V. M., Kuznetsov, V. A., Kurpatenkov, V. D., Obelnitsky, A. M., Poliaev, V. M., and Poliaev, B. I., *Osnoviy Teorii y Rascheta GRD (in Russian)*, Moskwa Visshaia Shkola, 1993.